

# Updating the Chandra HETGS Efficiencies using In-Orbit Observations

Herman L. Marshall<sup>a</sup>

<sup>a</sup>MIT Kavli Institute, Cambridge, MA, USA

## ABSTRACT

The efficiencies of the gratings in the High Energy Transmission Grating Spectrometer (HETGS) were updated using in-flight observations of bright continuum sources. The procedure first involved verifying that fluxes obtained from the +1 and -1 orders match, which checks that the contaminant model and the CCD quantum efficiencies agree. Then the fluxes derived using the high energy gratings (HEGs) were compared to those derived from the medium energy gratings (MEGs). The flux ratio was fit to a low order polynomial, which was allocated to the MEGs above 1 keV or the HEGs below 1 keV. The resultant efficiencies were tested by examining fits to blazar spectra.

**Keywords:** X-ray, spectrometer, calibration, grating

## 1. INTRODUCTION

This is an update to the *Chandra* High Energy Transmission Grating (HETG) calibration based on in-orbit observations. The HETG was described by Canizares et al. (2005 [1]) and previous flight calibration results were reported by Marshall et al. (2004 [2]). There are two grating types on the HETG: the high energy gratings (HEGs) have  $\times 2$  higher dispersion than the medium energy gratings (MEGs). When combined with the detectors, the system is called the HETG Spectrometer (HETGS).

A new set of HETG efficiencies was released as part of *Chandra* CalDB v4.4.7, which was intended to reduce systematic differences between the HEG and MEG fluxes as well as improve overall model fits. Here is provided details of the steps that went into the release and what is in store for the next update. Updates will also be available at the HETGS calibration web site <http://space.mit.edu/ASC/calib/hetgcal.html> and are presented regularly at meetings of the International Astronomical Consortium for High Energy Calibration (IACHEC) (see <http://web.mit.edu/iachec/meetings/index.html>).

## 2. DATA HANDLING

First, data were selected from the TGCat on-line catalog of HETGS spectra. See <http://tgcate.mit.edu> to obtain the data used here, which are given in Table 1. I started with sources of all sorts but relied most on extragalactic sources with relatively smooth continua. A simple type is given: “BLL” for the BL Lac objects (without strong optical emission lines), and “AGN” for the remaining quasars and Seyfert galaxies.

I follow an approach outlined in previous papers on HETGS effective area [2, 3]. For the  $i$ th observation with net counts  $C_i^+$  in the +1 order and  $C_i^-$  net counts in the -1 order and each grating, the ratio

$$R = \frac{Q_+ \sum_i C_i^-}{Q_- \sum_i C_i^+} \quad (1)$$

and its statistical uncertainty  $\sigma_R$  were computed over adaptively sized wavelength bins and a variety of sources. Note that the plus and minus order efficiencies are assumed to be equal, which is reasonable from ground tests and the random  $\pm 180^\circ$  installation of grating facets in the HETG. The detector QEs on the +1 and -1 sides,  $Q_+$  and  $Q_-$ , are derived from the models of the CCDs in the detector and depend on wavelength. Assuming that the QEs are not perfectly known,  $\hat{Q}_+$  and  $\hat{Q}_-$  are assigned to represent the *true* QEs on these sides, so that the expected counts in each wavelength bin on the +1 and -1 sides are given by

---

Further author information: (Send correspondence to H.L.M.)  
H.L.M.: hermanm@space.mit.edu, Telephone: 1 617 253 8573

Table 1. HETGS Calibration Observations

Name	Type	ObsID	Year	Exposure (ks)
3C 273	AGN	459	2000.30	38.6
PKS 2155-304	BLL	337	2000.38	38.6
ARK 564	AGN	863	2000.95	48.7
PKS 2155-304	BLL	1705	2001.33	25.5
MKN 509	AGN	2087	2001.65	57.9
3C273	AGN	2463	2001.82	26.7
PKS2155-304	BLL	1014	2002.07	26.7
NGC 4593	AGN	2089	2002.35	78.9
IC 4329A	AGN	2177	2002.42	59.1
3C273	AGN	3573	2002.58	29.7
3C 120	AGN	3015	2002.58	57.2
PKS2155-304	BLL	3167	2002.80	29.6
3C273	AGN	4430	2003.70	27.2
PKS2155-304	BLL	3708	2003.77	26.6
PKS2155-304	BLL	3706	2003.77	27.7
H 1426+428	BLL	3568	2003.90	99.4
3C273	AGN	5169	2005.38	29.7
PKS2155-304	BLL	5173	2005.57	26.7
3C382	AGN	4910	2005.62	54.2
3C382	AGN	6151	2005.72	63.9
1H1426+428	BLL	6088	2006.22	40.4
3C273	AGN	8375	2008.22	29.6
3C273	AGN	9703	2008.57	29.7
Ark 564	AGN	9898	2008.77	99.5
Ark 564	AGN	10575	2008.83	62.2
NGC 4051	AGN	10777	2009.00	27.4
NGC 4051	AGN	10775	2009.07	30.4
NGC 4051	AGN	10801	2009.23	25.7
Ark 564	AGN	9899	2009.42	84.1
MKN421	BLL	13098	2011.60	14.6

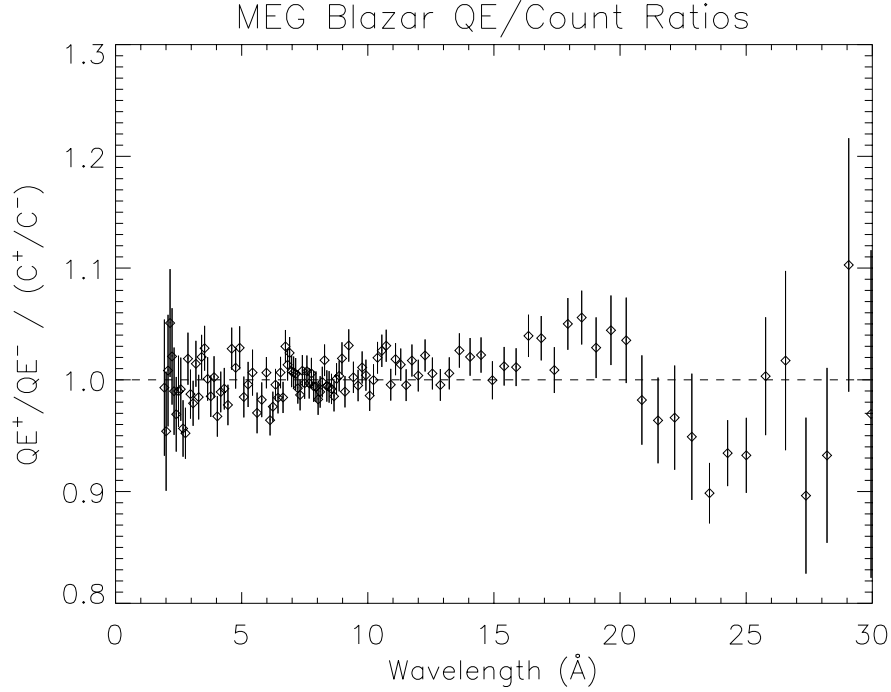


Figure 1. Ratio of adaptively binned MEG count rates from the +1 order to that of -1 order, corrected for the ratio of the quantum efficiencies of the detectors. The two sides agree to within 10% everywhere and to better than 3% over most energies. If the contaminant differed on the two sides, there would be a sharp edge at the O-K edge, 23.5 Å which is not observed.

$$C_i^+ = n_i A t_i \hat{\epsilon} T \hat{Q}_+ d\lambda \quad (2)$$

$$C_i^- = n_i A t_i \hat{\epsilon} T \hat{Q}_- d\lambda \quad (3)$$

where  $n_i$  is the source flux in  $\text{ph cm}^{-2} \text{s}^{-1} \text{Å}^{-1}$  for observation  $i$ ,  $A$  is the effective area of the HRMA,  $t_i$  is the observation exposure,  $\hat{\epsilon}$  is the true grating efficiency into first order for the grating of interest,  $T$  is the transmission of the detector filter,  $Q_+$  ( $Q_-$ ) is the CCD efficiency on the +1 (-1) order side, and  $d\lambda$  is the wavelength interval corresponding to one bin. All quantities are functions of wavelength except  $t_i$ . As defined, the quantity  $R$  is

$$R = \frac{Q_+ \hat{Q}_-}{Q_- \hat{Q}_+} \quad (4)$$

independent of the source model, grating efficiency, or filter transmission. The value of  $R$ , then, gives the ratio of true QEs relative to the modeled QEs. If we have reason to believe that the +1 QEs are correct, for instance, then  $Q_+ = \hat{Q}_+$ , so one may obtain the true -1 QE via  $\hat{Q}_- = RQ_-$  because  $R$  is observed and  $Q_-$  is the current QE model for the -1 side. See Fig. 1 for results. All fluxes came out to be consistent to within 1% on average except near 0.5 keV, where the two sides are consistent at the 3-5% level but generally within the uncertainties.

### 3. CORRECTING THE MEG/HEG EFFICIENCY RATIO

With a confirmation that the detector QEs on the +1 and -1 sides agree for both HEG and MEG, we now compare MEG to HEG. First, Eqs. 2 and 3 are recast to combine +1 and -1 orders:

$$C_i^H = C_i^{-H} + C_i^{+H} = n_i A t_i \hat{\epsilon}^H T(\hat{Q}_{-H} + \hat{Q}_{+H}) d\lambda \quad (5)$$

$$C_i^M = C_i^{-M} + C_i^{+M} = n_i A t_i \hat{\epsilon}^M T(\hat{Q}_{-M} + \hat{Q}_{+M}) d\lambda \quad (6)$$

Defining  $\hat{Q}_H = \hat{Q}_{-H} + \hat{Q}_{+H}$  and  $\hat{Q}_M = \hat{Q}_{-M} + \hat{Q}_{+M}$ , then we form the ratio

$$R_{M/H} = \frac{\epsilon_H \hat{Q}_H \sum_i C_i^M}{\epsilon_M \hat{Q}_M \sum_i C_i^H} \quad (7)$$

where, again, we assume that the grating efficiencies,  $\epsilon$ , are not perfectly known so that

$$R_{M/H} = \frac{\epsilon_H \hat{\epsilon}_M}{\epsilon_M \hat{\epsilon}_H} \quad (8)$$

gives the observed quantity that can be used to correct the MEG/HEG grating efficiency ratio. Again, as an example, if the HEG efficiencies are assumed to be correct, giving  $\epsilon_H = \hat{\epsilon}_H$ , then the observed values of  $R_{M/H}$  can be used to correct the MEG efficiencies by  $\hat{\epsilon}_M = \epsilon_M R_{M/H}$ . Note that  $\hat{Q}_H$  does not cancel  $\hat{Q}_M$  in eq. 7 because the ratio is obtained at the same wavelength for both MEG and HEG but will, in general, be on different detectors with different QEs due to the dispersion difference.

Results are shown in Fig. 2. Values are binned to have 1% uncertainties so that small systematic errors may be found and corrected; bins are required to be no wider than  $0.03\lambda$ . A 9th order polynomial was fit to the ratio data to create a correction factor,  $f$ , to apply to MEG efficiencies in order to force agreement between the MEG and HEG. At this point, one could equally well apply the correction to just HEG efficiencies, which would require multiplying them by  $1/f$ .

Fig. 3 shows the MEG/HEG flux ratio for a specific observation, obsID 3568 of the BLL source 1H 1426+428. The data clearly follow the trend fit to the average found from combining all observations; after correction, the residuals are random. A figure was generated for each source in order to search for irregularities in the MEG/HEG ratio but none were found in the data of the other targets.

### 4. ALLOCATING EFFICIENCY ADJUSTMENTS

Because the polynomial fit can correct only the ratio of the MEG and HEG efficiencies, the correction must be allocated to either the HEG or MEG efficiencies. The approach chosen was to pick a cross-over wavelength,  $\lambda_x$ ; for  $\lambda > \lambda_x$ , all corrections are applied to the HEG, while for  $\lambda < \lambda_x$ , the MEG efficiencies are corrected. The reasoning behind the choice is that it was somewhat easier to determine HEG efficiencies on the ground at high energies due to the higher resolution while harder to measure them at low energies due to significantly lower effective area. Furthermore, the HEG part of the HETGS dominates observations at high energy while the MEG part dominates at low energy, so a ‘‘least harm’’ dictum suggests applying less correction where a grating part dominates. Three values of  $\lambda_x$  were tried: 5.3 Å (2.3 keV), 10.8 Å (1.05 keV), and 17.7 Å (0.7 keV). The last choice effectively assigned the entire correction to the MEG.

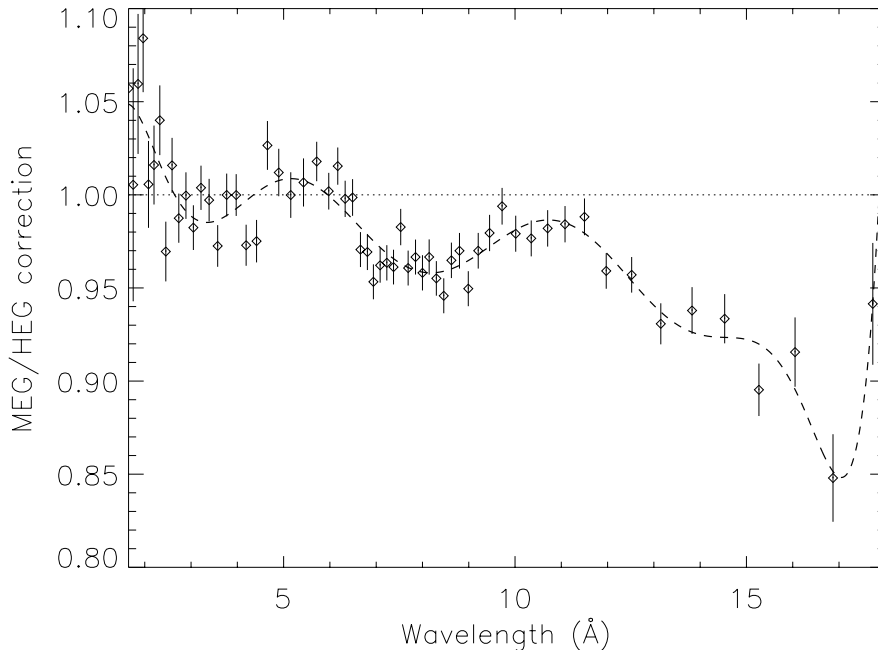


Figure 2. The ratio of the MEG and HEG fluxes as a function of wavelength, binned to have 1% uncertainties or bin widths less than 5% of the central wavelength. The sense of the correction is that the values shown should be applied to the MEG efficiencies to bring MEG fluxes into agreement with those derived from HEG data. The dashed line is a 9th order polynomial fit to the data.

## 5. SPECTRAL FIT RESULTS

The data for the sources in Table 1 were fit to several models to determine which sources have the smoothest spectra as a function of  $\lambda_x$ . Simple power law fits were tried first. All were found to have spectra approximating a simple power law but most showed significant spectral curvature. The BLL sources steepened to high energy while the AGN types generally flattened. This curvature can be described using a simple logarithmic parabola model with four parameters:

$$n_E = A e^{-N_H \sigma(E)} E^{-\Gamma + \beta \log E} \quad (9)$$

where  $N_H$  was fixed for each AGN to an estimate based on 21 cm data (the results are robust against the exact choice), and the overall model is a power law with a curvature term,  $\beta$ . The model is the same as that used for BL Lac objects by Perlman et al. (2005 [4]). The curvature term is negative for spectra that are convex upward and positive for those with soft or hard excesses. Fig. 4 shows two examples of fits to sources in the list.

Fig. 5 shows that the quality of the fit is related to the value of  $\beta$ : better fits are obtained for negative curvature. The fits with positive curvature were predominantly radio-loud AGN with optical emission lines, indicating that these spectra are actually more complex than a simply curving model provides. For the remaining analysis, the sources with  $\beta < 0.3$  were chosen; these were the BL Lac objects PKS 2155-304 and 1H 1426-428. The curvature values are similar to those found for other BL Lac objects [4].

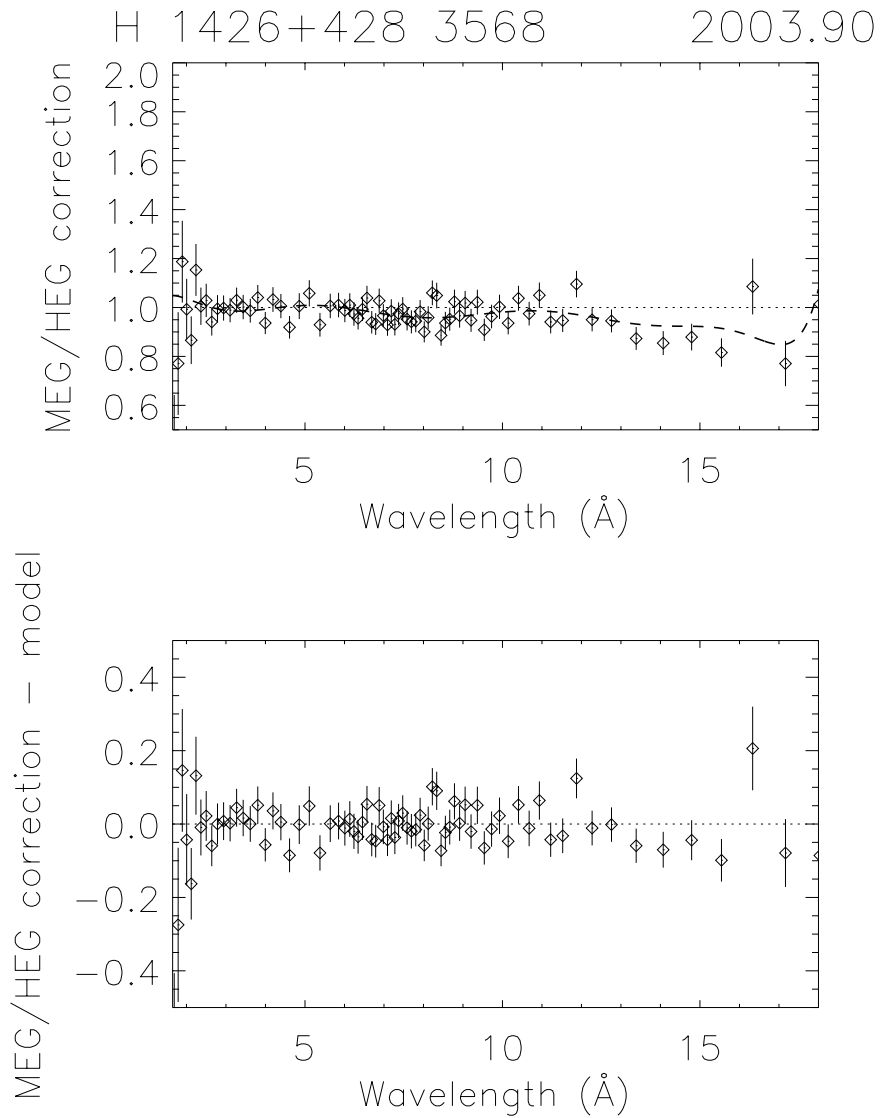


Figure 3. Test of the HEG/MEG corrections on one blazar, the BL Lac object 1H 1426+428, from obsID 3568, observed late in 2003. The top panel shows the original ratio data and the spline fit from Fig. 2. The bottom panel shows the residuals after correction, which are consistent with zero.

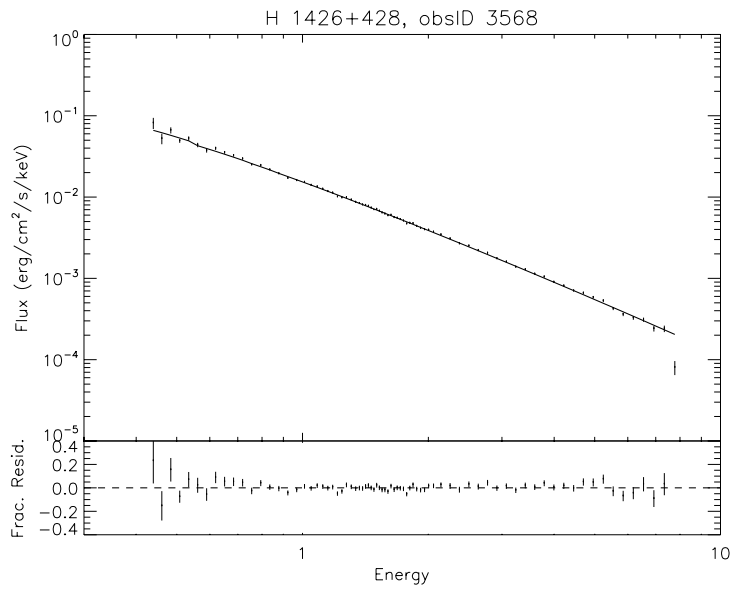
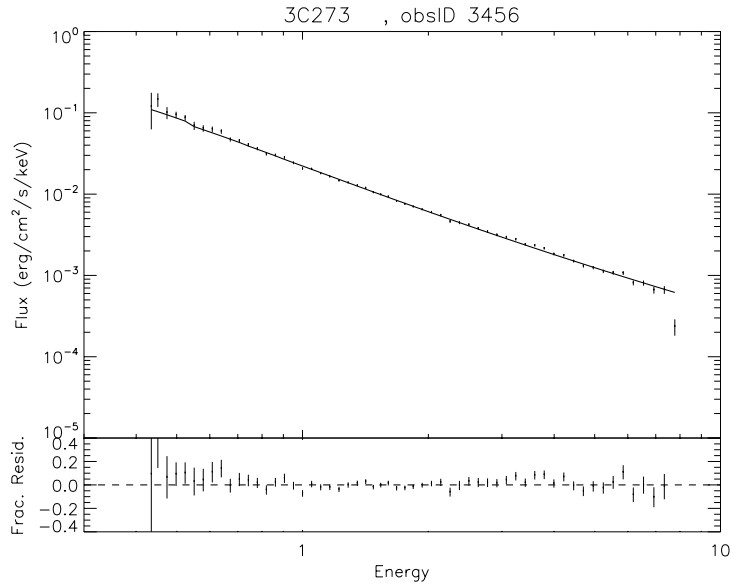


Figure 4. Examples of spectral fits using eq. 9 for two sources, the radio loud quasar 3C 273 (obsID 3456, top) and the BL Lac object 1H 1426+428 (obsID 3568, bottom). The top panel shows the flux density and the fit and the bottom panel shows the residuals. Both are very well modeled by a power law with a slight curvature. In the case of 3C 273, there is positive curvature due to the soft excess and a possible reflection component or broadened Fe-K line. In this case, the reduced  $\chi^2$  is over 2. For 1H 1426+428, the model fits much better and curves downward to high energies.

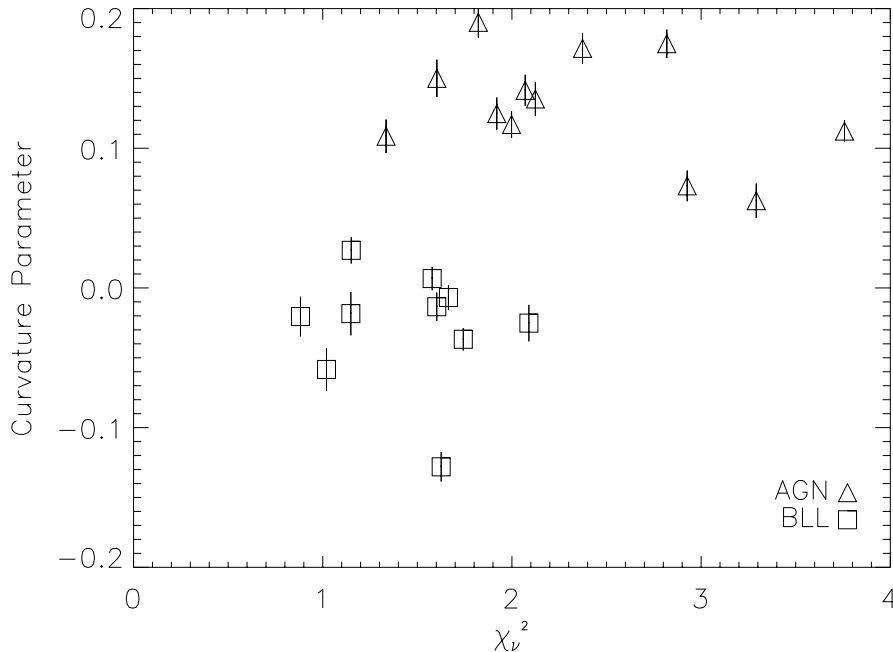


Figure 5. The curvature parameter  $\beta$ , as a function of reduced  $\chi^2$  for fits to HETGS spectra from Table 1. See Eq. 9 for the model, which defines  $\beta$ , the curvature parameter. The BLL type sources fit the model best and generally have negative curvatures, so that their spectra steepen with energy. The AGN, such as 3C 273, have more complex spectra that include a soft excess. For these fits, the cross-over wavelength was set to 10.3Å.

## 6. DETERMINING THE CROSS-OVER WAVELENGTH

By fitting simple power law spectra to the BLL sources in the list, one may argue against the extreme values of  $\lambda_x$ . The average reduced  $\chi^2$ ,  $\chi_\nu^2$ , for the BLL sources was smallest for  $\lambda_x = 10.8\text{\AA}$ , at 1.40; for  $\lambda_x = 5.3\text{\AA}$ , the average  $\chi_\nu^2$  was 2.78, and for  $\lambda_x = 17.7\text{\AA}$ , the average  $\chi_\nu^2$  was 1.68. Thus, choosing a cross-over near 1 keV provides the smoothest spectra. A schematic of how the MEG/HEG ratio correction is allocated is shown in Fig. 6.

The spectral residuals for the BL Lac objects were combined in order to see if there were significant remaining residuals that could be corrected. Fig. 7 shows the result. At this point, the residuals are in the range of  $\pm 3 - 5\%$  over most of the HETGS energy range and show no particular pattern that could be readily corrected.

## 7. CONCLUSION

While there are possible systematic errors of up to 5% over the 0.5-7 keV range, most of the deviations are less than 3% (Fig. 7). Residuals to simple fits to the other AGN (not shown) are also less than 3% over most of the 0.5-7% range and only as large as 5% near 0.7 keV. Thus, an approximate limit to relative systematic errors is about 3-5% over the HETGS range. While these residual errors will be examined further to see if they can be eliminated, another area of investigation will be the cross-dispersion selection efficiency, which is currently applied in the grating RMFs.



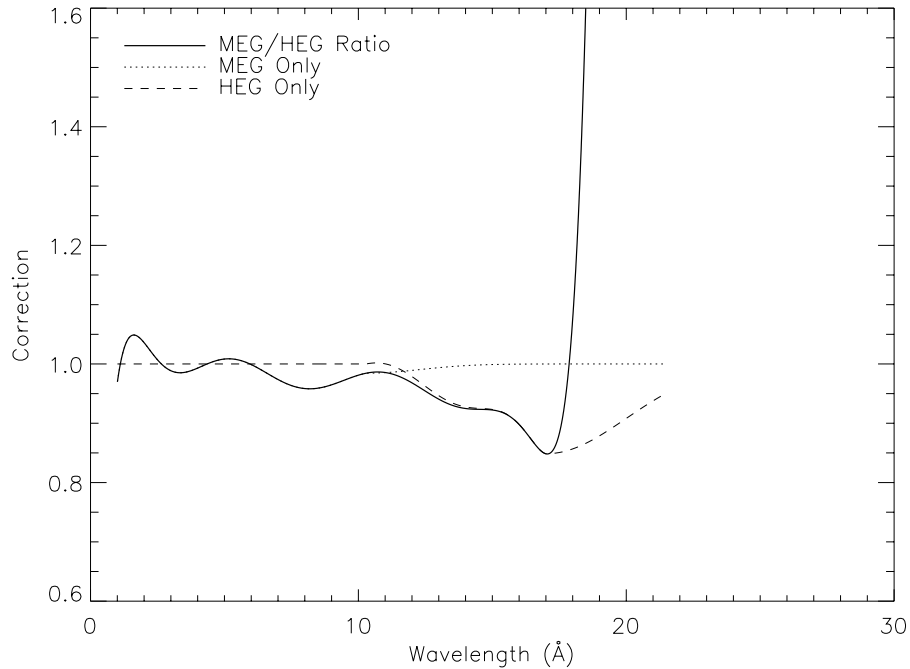


Figure 6. Apportioning the MEG/HEG ratio correction. The correction was divided into two parts. Below 12 Å, it is allocated to the MEG, while above 12 Å, it is allocated primarily to the MEG. The correction to the HEG efficiency is actually the inverse of that shown, so that it matches the expected total correction near 15 Å. The HEG correction tails off to unity longward of 17 Å due to the lack of data that causes the spline fit to extrapolate badly.

### ACKNOWLEDGMENTS

Support for this work was provided by the National Aeronautics and Space Administration (NASA) through the Smithsonian Astrophysical Observatory (SAO) contract SV3-73016 to MIT for support of the Chandra X-Ray Center (CXC), which is operated by SAO for and on behalf of NASA under contract NAS8-03060.

### References

- [1] Canizares, C.R., et al., 2005, *PASP*, 117, 1144.
- [2] Marshall, H. L., Dewey, D., & Ishibashi, K. 2004, *Proceedings SPIE*, 5165, 457
- [3] Marshall, H. L., Dewey, D., Schulz, N. S., & Flanagan, K. A. 1998, *Proceedings SPIE*, 3444, 64
- [4] Perlman, E. S., et al. 2005, *ApJ*, 625, 727

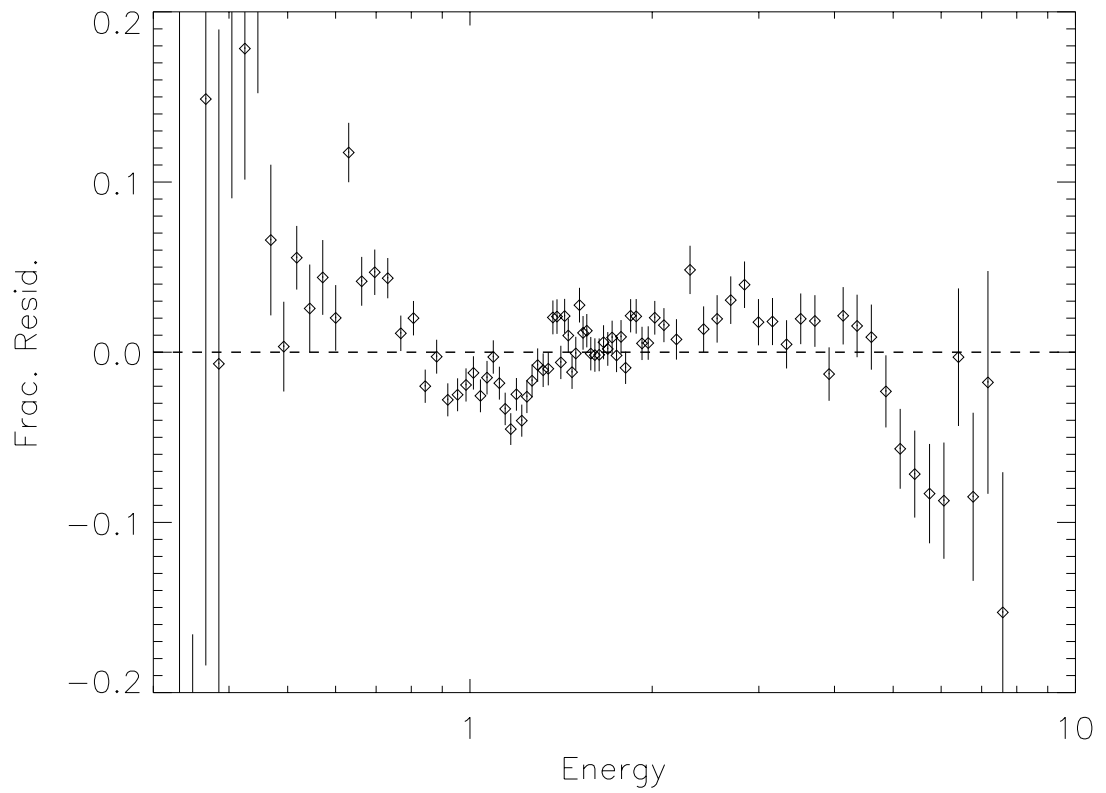


Figure 7. The average residuals for curved power law fits to the HETGS data for BL Lac objects. For most of the HETGS range, the systematic deviations are not significant or are less than 3%. Deviations of 5-10% near 6 keV and 0.7 keV will be investigated further.